

Cite this: *J. Mater. Chem. A*, 2021, 9, 2683Received 23rd July 2020
Accepted 11th January 2021

DOI: 10.1039/d0ta07207a

rsc.li/materials-a

Guest-tuned proton conductivity of
a porphyrinylphosphonate-based hydrogen-
bonded organic framework†Yijie Wang,^a Jianbo Yin,^a Di Liu,^a Chengqi Gao,^a Zixi Kang,^b Rongming Wang,^c Daofeng Sun[†] and Jianzhuang Jiang[†]

Hydrogen-bonded organic frameworks (HOFs), similar to their MOF analogues, exhibit great potential in proton conduction applications. Herein, a porous HOF namely [(NiH₄TPPP)(Me₂NH₂)₄(DMF)(H₂O)₄] (UPC-H5) was synthesized from phosphonate-based porphyrinato nickel (NiH₄TPPP), and its proton conductivity is regulated through a two-step guest change. Firstly, immersing UPC-H5 in CH₂Cl₂ to exchange lattice solvent molecules for 24 h followed by heating under vacuum afforded the lattice solvent molecule-free HOF [(NiH₄-TPPP)(Me₂NH₂)₄] (UPC-H5a) with the pristine framework still retained. Secondly, exposing UPC-H5a to vapors of 25% aqueous ammonia for 24 h at room temperature gave a new derivative UPC-H5a@NH₃·H₂O with the molecular formula [(NiH₄TPPP)(Me₂NH₂)₂(NH₄)₂(H₂O)₄] according to elemental and thermal analyses. At 30 °C and 95% R.H., the proton conductivity of UPC-H5, UPC-H5a, and UPC-H5a@NH₃·H₂O amounts to 5.59 × 10⁻⁴, 7.00 × 10⁻³, and 1.47 × 10⁻² S cm⁻¹, respectively, which increases to 1.85 × 10⁻³, 3.42 × 10⁻², and 1.59 × 10⁻¹ S cm⁻¹ at 80 °C and 99% R.H., clearly showing the effect of guest regulation on the proton conductivity of the HOF-based materials. In addition, this result is also helpful towards understanding the important role of guests in the formation of their proton conduction pathways.

With the increasing consumption of fossil energy, humankind is facing not only the energy depletion situation but also environmental pollution.¹ Over the past few decades, great efforts have been devoted to developing new clean and renewable

energy sources such as nuclear energy, solar energy, geothermal energy, hydropower, and hydrogen energy.² Among them hydrogen seems to be an ideal candidate to resolve the corresponding problems because of its abundance, high energy density, and environmentally benign combustion product.³ As a consequence, fuel cell technologies in particular proton exchange membrane fuel cells (PEMFCs) that are able to utilize hydrogen as a raw material have been recognized as a crucial solution to alternative energy sources due to their high efficiency and low emission.⁴ Among the important components constituting PEMFCs, the proton exchange membrane (PEM) plays a key role in the cell's performance enhancement. Therefore, developing efficient and stable proton conducting materials suitable for PEMs has been one of the important research topics in this field.⁵

Nafion and Nafion-like polymers showing excellent proton conducting properties have been employed as proton exchange membranes for PEMFCs. However, some disadvantages of these organic polymers including fabrication difficulty, narrow working conditions, and high cost restrict their further wide range of applications. In particular, their amorphous nature prevents researchers from clearly understanding the structure-property relationship as well as the proton conduction mechanism. This in turn limits further optimization over their proton conduction pathways through a rational manner.⁶ In the past two decades, rapidly developing crystalline solid materials, metal organic frameworks/coordination polymers (MOFs/CPs),⁷ and covalent organic frameworks (COFs)⁸ have shown great application potential in proton conduction. Their highly ordered and well-defined porous structures are very helpful in investigating and understanding the proton conduction mechanism towards further improving their proton conductivity.⁹ Thus far, three main strategies have been revealed and employed to improve the proton conductivity of MOFs and COFs on the basis of chemical modification over either precursors or frameworks: (1) introducing acidic groups such as -COOH, -SO₃H, and -PO₃H₂ into the framework to improve the proton density of materials;^{9e,10} (2) introducing a conducting

^aCollege of Science, China University of Petroleum (East China), Qingdao, Shandong 266580, China. E-mail: rrmwang@upc.edu.cn; dfsun@upc.edu.cn

^bState Key Laboratory of Heavy Oil Processing, School of Materials Science and Engineering, China University of Petroleum (East China), Qingdao, Shandong 266580, People's Republic of China

^cBeijing Key Laboratory for Science and Application of Functional Molecular and Crystalline Materials, Department of Chemistry, University of Science and Technology Beijing, Beijing 100083, China. E-mail: jianzhuang@ustb.edu.cn

† Electronic supplementary information (ESI) available: Synthetic details, FTIR images, PXRD patterns, TGA results, etc. CCDC 1976307. For ESI and crystallographic data in CIF or other electronic format see DOI: 10.1039/d0ta07207a

medium such as water, N-heterocyclic compounds, and H_3PO_4 to improve the proton carrier density in the pores or channels;¹¹ (3) tuning the hydrogen bonded networks to optimize the proton transfer pathways.¹² It is however worth noting that thus far most excellent MOF- and COF-based proton conductors with high proton conductivity employ water as the proton-conducting medium depending on the degenerate conjugate acid–base system ($\text{H}_2\text{O} + \text{H}_3\text{O}^+ \rightleftharpoons \text{H}_3\text{O}^+ + \text{H}_2\text{O}$ or $\text{H}_2\text{O} + \text{OH}^- \rightleftharpoons \text{OH}^- + \text{H}_2\text{O}$).^{9f,13} In good contrast, ammonia-mediated proton conducting MOF/COF materials still remain rarely reported, despite the recent demonstration of ammonia as an excellent proton-conducting medium depending on conjugate acid–base proton transfer ($\text{NH}_4^+ + \text{NH}_3 \rightleftharpoons \text{NH}_3 + \text{NH}_4^+$) reported by Kitagawa and co-authors.¹⁴

As the counterparts of MOFs and COFs, hydrogen bonded organic frameworks (HOFs) that are constructed mainly depending on hydrogen-bond interactions have also shown great application potential in diverse fields including gas storage and separation,¹⁵ catalysis,¹⁶ molecular recognition,¹⁷ and chemical sensing.¹⁸ As can be expected, efforts have also been made towards exploring the proton conducting properties of this kind of material.¹⁹ In this work, we report the fabrication and proton conduction properties of a porous porphyrin-based HOF, $[(\text{NiH}_4\text{TPPP})(\text{Me}_2\text{NH}_2)_4(\text{DMF})(\text{H}_2\text{O})_4]$ (UPC-H5, $\text{NiH}_8\text{-TPPP}$: 5,10,15,20-tetrakis(4-phosphonophenyl) porphyrin nickel(II), Me_2NH : dimethylamine, DMF: *N,N*-dimethylformamide). The proton conductivity of the HOF-based material could be further regulated through a two-step guest-tuned strategy, Scheme S1.† First, removing the lattice DMF molecules that cannot form hydrogen bond networks in the channels of the framework to accommodate more guest water molecules to form more smoother proton-conducting pathways; second, partially replacing the Me_2NH_2^+ moieties with a larger volume and higher $\text{p}K_a$ value (10.75) with NH_4^+ with a smaller volume and lower $\text{p}K_a$ value (9.26) to increase the pore volume and hydrophilicity of channels also to form more and smoother proton-conducting pathways with guest water molecules. Such a two-step guest regulation provides about two orders of magnitude increase in the proton conductivity.

UPC-H5 was prepared by the assembly of NiH_8TPPP in the mixed solution of acetone, DMF, and H_2O . According to single-crystal X-ray diffraction structural analysis, UPC-H5 crystallizes in a triclinic $P\bar{1}$ space group, Table S1.† The asymmetric unit contains one $\text{NiH}_4\text{TPPP}^{4-}$, four Me_2NH_2^+ , one lattice DMF, and four lattice water molecules. As shown in Fig. 1, each $\text{NiH}_4\text{-TPPP}^{4-}$ provides four H atoms from four $-\text{PO}_3\text{H}$ groups and accepts four H atoms of four $-\text{PO}_3\text{H}$ groups to form eight $\text{O}-\text{H}\cdots\text{O}$ hydrogen bonds with six surrounding $\text{NiH}_4\text{TPPP}^{4-}$ building blocks, leading to the formation of a two-dimensional (2D) hydrogen-bonded network containing two layers of $\text{NiH}_4\text{-TPPP}^{4-}$ with $\pi-\pi$ interactions (3.67 Å), Fig. 1b and c. Meanwhile, the eight hydrogen bonds include four types of $\text{O}3-\text{H}3\cdots\text{O}11$, $\text{O}5-\text{H}5\cdots\text{O}7$, $\text{O}8-\text{H}8\cdots\text{O}4$, and $\text{O}10-\text{H}10\cdots\text{O}9$ with the $\text{O}\cdots\text{O}$ distances of 2.54, 2.56, 2.47 and 2.60 Å, respectively and the bond angles of 170°, 166°, 175° and 166°, Table S2.† and Fig. 1d. Then a stable 3D structure is further formed depending on the hydrogen-bonding and electrostatic interactions among

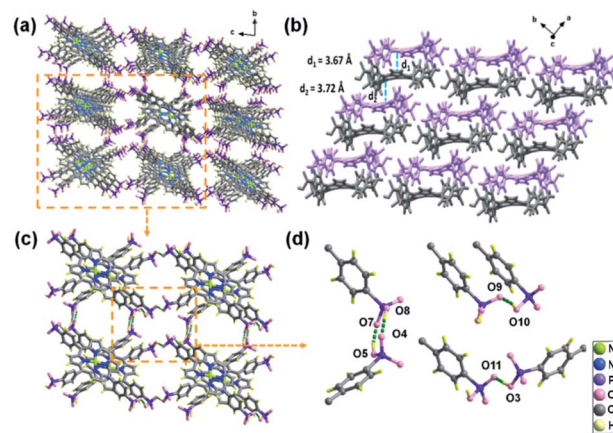


Fig. 1 Crystal structure of UPC-H5. (a) 3D anionic framework formed by $\text{NiH}_4\text{TPPP}^{4-}$ showing 1D channels, Me_2NH_2^+ , DMF and H_2O are omitted for clarity; (b) the stacking of 2D layers showing the distances of $\pi-\pi$ interactions; (c) the local enlarged 2D layers; (d) four types of hydrogen bonds between $\text{NiH}_4\text{TPPP}^{4-}$.

the 2D layers, Me_2NH_2^+ moieties and lattice water molecules under the assistance of $\pi-\pi$ interactions (3.72 Å), Fig. 1b. When viewed along the a axis, UPC-H5 possesses three different sizes of 1D channels. The biggest sized channel scales 11.0827 Å (benzyl C–C) \times 11.3948 Å (phosphonate O–O), in which the lattice DMF molecules exist. The medium- and smallest-sized channels are of the scale 9.8735 Å (benzyl C–C) \times 10.3008 Å (phosphonate O–O) and 5.8385 Å (phosphonate O–O) \times 7.9652 Å (phosphonate O–O), in which Me_2NH_2^+ and lattice water molecules reside, respectively, Fig. 1a. The total solvent-accessible volume of UPC-H5 is calculated to be 33.2% according to the SQUEEZE module of the PLATON routine.²⁰ After immersing UPC-H5 in CH_2Cl_2 to exchange lattice solvent molecules for 24 h followed by heating under vacuum, $[(\text{NiH}_4\text{-TPPP})(\text{Me}_2\text{NH}_2)_4]$ (UPC-H5a) was obtained. UPC-H5a was then exposed to vapors of 25% aqueous ammonia for 24 h at room temperature, giving UPC-H5a@ $\text{NH}_3\cdot\text{H}_2\text{O}$.

As shown in Fig. S1,† the powder X-ray diffraction (PXRD) pattern of the as-synthesized UPC-H5 is in good agreement with the one simulated from the single crystal diffraction data, revealing the high phase purity of the freshly prepared samples. This is further supported by the elemental analysis result as listed in the ESI.† The PXRD pattern of UPC-H5a does not show significant changes in comparison with that for UPC-H5, except for the slight shift of the peak at 5.7° to 6.0°, indicating the slight shrink of the fundamental HOF framework after losing the lattice DMF and water molecules in UPC-H5. This, however, is not the case for UPC-H5a@ $\text{NH}_3\cdot\text{H}_2\text{O}$. A big change in the PXRD pattern of UPC-H5a@ $\text{NH}_3\cdot\text{H}_2\text{O}$, Fig. S1,† reveals the significant transformation occurring in the framework structure. However, the framework remains uncollapsed as shown in its PXRD analysis, and the crystal shape of UPC-H5a@ $\text{NH}_3\cdot\text{H}_2\text{O}$ has no change compared with that of UPC-H5. In addition, the *in situ* PXRD analysis discloses that the structures of UPC-H5, UPC-H5a, and UPC-H5a@ $\text{NH}_3\cdot\text{H}_2\text{O}$ show good stability up to 120 °C, Fig. S2.† Correspondingly, TG-MS analyses indicate that

UPC-H5 loses 5.8% weight from room temperature to 120 °C, which is attributed to the loss of four lattice water molecules (calculated value 5.5%), and then Me_2NH_2^+ ions begin to decompose along with the loss of lattice DMF molecules. UPC-H5a shows almost no weight loss below 125 °C because of the lack of lattice solvents. The structure, however, slowly gets collapsed after that along with the decomposition and loss of Me_2NH_2^+ . In contrast, UPC-H5a@ $\text{NH}_3 \cdot \text{H}_2\text{O}$ loses 6.7% weight from room temperature to 95 °C, corresponding to the loss of about four water molecules (calculated value 6.1%), and then NH_4^+ and Me_2NH_2^+ ions begin to decompose, Fig. S3.† In combination with the elemental analysis result listed in the ESI,† the molecular formula of UPC-H5a@ $\text{NH}_3 \cdot \text{H}_2\text{O}$ is speculated to be $[(\text{NiH}_4\text{TPPP})(\text{Me}_2\text{NH}_2)_2(\text{NH}_4)_2(\text{H}_2\text{O})_4]$. That is to say, about two Me_2NH_2^+ moieties in UPC-H5a are replaced by two NH_4^+ moieties in every structural unit of UPC-H5a@ $\text{NH}_3 \cdot \text{H}_2\text{O}$, and four water molecules re-enter the channels during the ammonia-exchange process of UPC-H5a.

To further clarify the structures of UPC-H5, UPC-H5a, and UPC-H5a@ $\text{NH}_3 \cdot \text{H}_2\text{O}$, their infrared spectra were recorded and are shown in Fig. S4.† Compared with NiH_8TPPP , UPC-H5 exhibits a C=O characteristic vibration peak of lattice DMF molecules at 1661 cm^{-1} , a C-H bending vibration of Me_2NH_2^+ at 1469 cm^{-1} , and a C-N stretching vibration of Me_2NH_2^+ peak at 1050 cm^{-1} , well consistent with the single crystal X-ray analysis result. However, the peak at 1661 cm^{-1} disappeared in the IR spectrum of UPC-H5a, indicating the complete removal of the lattice DMF. As can be found, a new peak belonging to the N-H bending vibration of NH_4^+ appears at 1634 cm^{-1} in the IR spectrum of UPC-H5a@ $\text{NH}_3 \cdot \text{H}_2\text{O}$, demonstrating the partial replacement of Me_2NH_2^+ by NH_4^+ .

To assess the permanent porosity of UPC-H5a and UPC-H5a@ $\text{NH}_3 \cdot \text{H}_2\text{O}$, both samples after CH_2Cl_2 exchange were activated to eliminate lattice solvents by heating at 80 °C for 24 h under vacuum. Then gas uptake tests were conducted at different temperatures. Because of the hydrophilic characteristics of the channels with a large number of $-\text{PO}_3\text{H}$ and $-\text{NH}$ groups, both materials absorb only a small amount of N_2 under a high pressure even at 77 K, Fig. S5.† However, they can adsorb 99 and $131 \text{ cm}^3 \text{ g}^{-1}$ of CO_2 at 196 K, Fig. S6.† The total pore volume is then calculated to be 0.18 and $0.23 \text{ cm}^3 \text{ g}^{-1}$, respectively, with the Brunauer-Emmett-Teller surface areas of 237.5 and $371.1 \text{ m}^2 \text{ g}^{-1}$, according to the CO_2 isotherm ($P/P_0 = 0.98$), Fig. S7.† These results indicate that UPC-H5a@ $\text{NH}_3 \cdot \text{H}_2\text{O}$ keeps the porosity after ammonia-exchange, but actually possesses larger porosity and specific surface area than UPC-H5a despite the significant structural change. In addition, the water adsorption isotherms of three HOFs were recorded at 298 K after removing lattice water and free water molecules that may be adsorbed in air. As shown in Fig. S8, UPC-H5, UPC-H5a and UPC-H5a@ $\text{NH}_3 \cdot \text{H}_2\text{O}$ can take up ca. 3.5, 4.8, and 7.7 water molecules at 40% RH, and ca. 4.8, 8.7, and 16.4 water molecules at 85% RH, and rapidly increase to ca. 9.3, 14.3 and 29.4 water molecules per formula unit at 94% RH, respectively. This indicates that both the removal of DMF and ammonia-exchange have bigger influence on the water adsorption capacity under higher humidity, and means that UPC-H5 can take up 5 water

molecules at 94% RH on the basis of the initial 4 lattice water molecules, and UPC-H5a can adsorb 5 more water molecules after removing DMF molecules. Compared with UPC-H5a, UPC-H5a@ $\text{NH}_3 \cdot \text{H}_2\text{O}$ can take up 15 more water molecules because part of Me_2NH_2^+ is replaced by NH_4^+ , resulting in a bigger pore volume and stronger hydrophilicity.

The proton conduction performance of UPC-H5, UPC-H5a, and UPC-H5a@ $\text{NH}_3 \cdot \text{H}_2\text{O}$ was explored by the impedance technique using their pressed pellets under different relative humidities (R.H.) (from 40 to 99%). Towards revealing the guest-tuned effect, the proton conductivity of these materials was studied under exactly the same testing conditions. At first, the time-dependent proton conductivity was calculated (Fig. S9†), showing that the equilibrium time of UPC-H5, UPC-H5a and UPC-H5a@ $\text{NH}_3 \cdot \text{H}_2\text{O}$ is almost 170, 120, and 100 minutes at 80 °C and 40% R.H., and 100, 80, and 70 minutes at 80 °C and 99% R.H., respectively. As shown in Fig. S10 and Table S3,† UPC-H5 shows only a low proton conductivity of $1.04 \times 10^{-6} \text{ S cm}^{-1}$ at 25 °C and under 40% R.H., indicating its relatively weak active proton conducting nature under low temperature and humidity conditions, based on the hydrogen-bonding networks formed by $-\text{PO}_3\text{H}$, Me_2NH_2^+ , and H_2O along the *a* and *b* axes, Fig. S11.†^{9b-f} Also at 25 °C and under 40% R.H., the conductivity of UPC-H5a and UPC-H5a@ $\text{NH}_3 \cdot \text{H}_2\text{O}$ was found to be 8.23×10^{-6} and $1.68 \times 10^{-5} \text{ S cm}^{-1}$, respectively, indicating the slight influence of eliminating the lattice DMF molecules in UPC-H5 and ammonia-exchange in UPC-H5a@ $\text{NH}_3 \cdot \text{H}_2\text{O}$ on their proton conduction performance under low humidity, because UPC-H5a and UPC-H5a@ $\text{NH}_3 \cdot \text{H}_2\text{O}$ can take up ca. 1.3 and 2.9 more water molecules than UPC-H5 under these conditions, respectively. With increasing the humidity to 99% R.H., the proton conductivity of UPC-H5, UPC-H5a, and UPC-H5a@ $\text{NH}_3 \cdot \text{H}_2\text{O}$ at 25 °C increases to 4.28×10^{-4} , 6.24×10^{-3} , and $1.39 \times 10^{-2} \text{ S cm}^{-1}$, respectively. This is also consistent with the results of water adsorption experiments that they can adsorb more water molecules under higher humidity, showing the important role of water in the construction of proton transfer pathways.

With the increasing of temperature, the proton conductivity of UPC-H5 increases to $9.28 \times 10^{-6} \text{ S cm}^{-1}$ at 40 °C and 40% RH, and $4.68 \times 10^{-5} \text{ S cm}^{-1}$ at 80 °C and 40% RH, Fig. 2, S12 and Table S4.† Correspondingly, UPC-H5a exhibits a proton conductivity of $5.22 \times 10^{-5} \text{ S cm}^{-1}$ at 80 °C and 40% RH. Interestingly, ammonia-exchange shows an obvious influence on enhancing the proton conductivity, increasing the proton conductivity of UPC-H5a@ $\text{NH}_3 \cdot \text{H}_2\text{O}$ to $1.43 \times 10^{-3} \text{ S cm}^{-1}$ at 80 °C and under 40% R.H., an almost two orders of magnitude increase. As shown in Fig. 2, along with increasing the humidity to 99% R.H., the proton conductivity of UPC-H5, UPC-H5a, and UPC-H5a@ $\text{NH}_3 \cdot \text{H}_2\text{O}$ at 80 °C gets increased in a rapid manner to 1.85×10^{-3} , 3.42×10^{-2} , and $1.59 \times 10^{-1} \text{ S cm}^{-1}$, respectively, further disclosing the important role of water in the construction of proton transfer pathways. As can be seen, at 80 °C and under 99% R.H., the conductivity of UPC-H5a amounts to about 18 times higher than that for UPC-H5, suggesting the increased influence of eliminating the lattice DMF molecules of UPC-H5 on the proton conduction performance

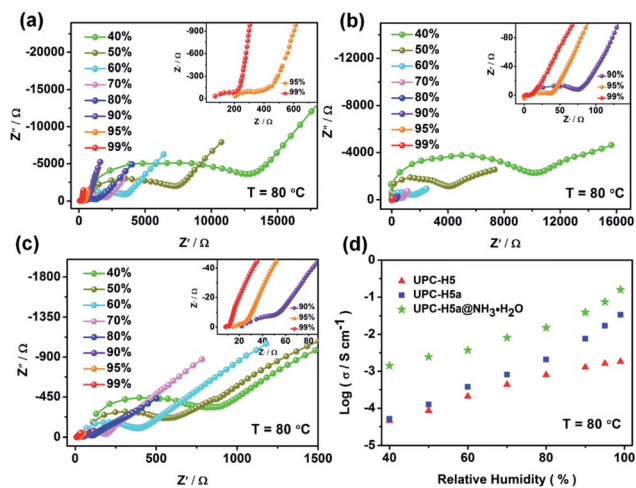


Fig. 2 Nyquist plots of UPC-H5 (a), UPC-H5a (b) and UPC-H5a@NH₃·H₂O (c) at 80 °C under different R.H. values; and the humidity-dependent proton conductivity of UPC-H5, UPC-H5a and UPC-H5a@NH₃·H₂O (d).

under high humidity. Similar to the low humidity situation, the proton conductivity of UPC-H5a@NH₃·H₂O still remains almost two orders of magnitude higher than that for UPC-H5 under 99% R.H., confirming the significant role of ammonia-exchange. Meanwhile, six cyclic tests were carried out to measure the proton conductivities of UPC-H5, UPC-H5a, and UPC-H5a@NH₃·H₂O between 40% and 99% R.H. at 80 °C, showing a negligible change in the conductivity values, indicating their good structure and property stability under the testing conditions, Fig. S13.† In order to further verify the structural stability of UPC-H5a@NH₃·H₂O, its crystals and pellet were placed at 80 °C and 99% R.H. for one week. The EDS elemental mapping images of the UPC-H5a@NH₃·H₂O crystals before and after placing do not show an obvious change, demonstrating their long-term structural stability at 80 °C and 99% R.H., Fig. S14.† Moreover, the proton conductivity of the UPC-H5a@NH₃·H₂O pellet was measured every day for one week, and the conducting values remained well consistent, indicating that it also has good long-term property stability under these conditions, Fig. S15.† At the end of this section, it is worth noting that these results clearly show the guest-tuned effect on the proton conductivity of HOF-based materials for the first time. Meanwhile, the proton conductivity of UPC-H5a@NH₃·H₂O ranks as one of the highest values among the excellent porous proton-conducting materials reported to date, Table S5.†

To further understand the relationship between proton conductivity and temperature, the temperature-dependent proton conductivity of UPC-H5, UPC-H5a, and UPC-H5a@NH₃·H₂O was also tested under 95% R. H. in a varying temperature range from 30 to 80 °C. As displayed in Fig. 3 and Table S6,† the conductivity of UPC-H5, UPC-H5a, and UPC-H5a@NH₃·H₂O at 30 °C and 95% R.H. is 5.59×10^{-4} , 7.00×10^{-3} , and 1.47×10^{-2} S cm⁻¹, respectively, verifying the effectiveness of regulating guests on the proton conduction

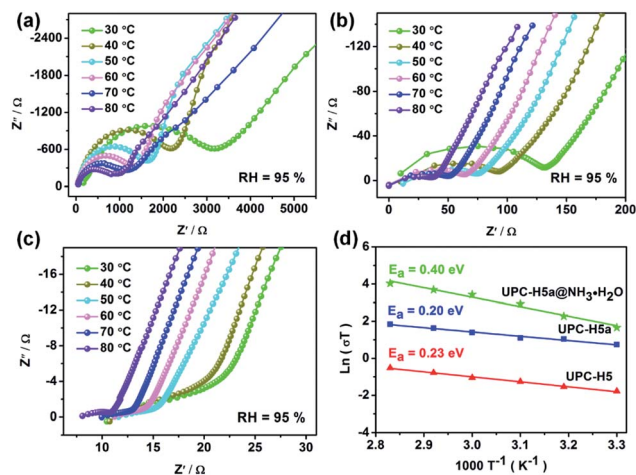


Fig. 3 Nyquist plots of UPC-H5 (a), UPC-H5a (b) and UPC-H5a@NH₃·H₂O (c) under 95% R.H. at different temperatures; and Arrhenius plots of UPC-H5, UPC-H5a and UPC-H5a@NH₃·H₂O at 80 °C and under 95% R.H. (d).

performance even at ambient temperature under high humidity. With increasing the temperature, the conducting values increase gradually and reach 1.71×10^{-3} , 1.82×10^{-2} , and 8.68×10^{-2} S cm⁻¹ at 80 °C and 95% R.H., respectively. Obviously, the effect of temperature on proton conductivity is much smaller than that of humidity as detailed above. According to the Arrhenius equation, activation energies (E_a) of 0.23, 0.20, and 0.40 eV for UPC-H5, UPC-H5a, and UPC-H5a@NH₃·H₂O were obtained by fitting the temperature-dependent conductivity data, suggesting their possible Grotthuss transport mechanism. In addition, we also carried out five contrasting tests using five different pellets for measuring the temperature-dependent proton conductivity of each sample at 95% R.H. As exhibited in Fig. S16,† the conducting values remain consistent in a good manner for different pellets, indicating their good proton conductivity reproducibility. Besides, the PXRD patterns before and after the cyclic temperature- and humidity-dependent impedance tests for UPC-H5, UPC-H5a and UPC-H5a@NH₃·H₂O do not show an obvious change, Fig. S17,† indicating their structural stability.

As can be seen, despite the existence of a high density of $-\text{PO}_3\text{H}$, Me_2NH_2^+ , and H_2O in the channels, the proton conductivity of UPC-H5 is still poor under low humidity, suggesting that the proton conduction of UPC-H5 did not mainly originate from its intrinsic hydrogen bond networks but from the free water molecules which enter the channels to reorganize the proton transfer pathways. However, the existence of lattice DMF molecules in UPC-H5 greatly hinders the free water molecules from entering the channels, Fig. 4a. As a result of removing the lattice molecules, free water molecules can enter the empty type III channels in UPC-H5a to form more proton conduction pathways, in addition to entering the types I and II channels just the same as in UPC-H5, Fig. 4b, S11, and S18,† inducing an improved proton conducting performance. However, the methyl groups of Me_2NH_2^+ in UPC-H5a still block the formation of better hydrogen bond networks in multiple

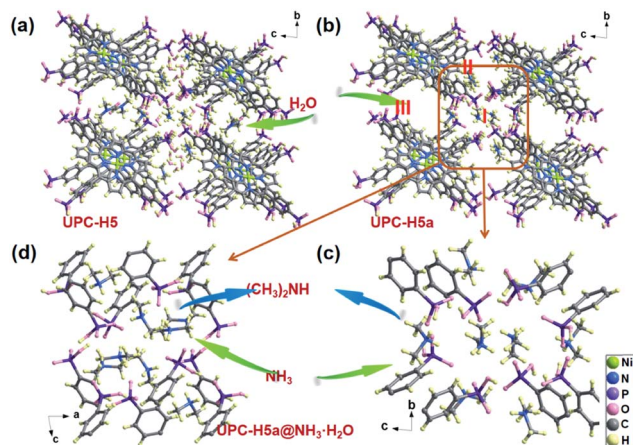


Fig. 4 (a and b) The structures showing the guests viewed along the *a* axis for UPC-H5 and UPC-H5a, respectively; (c and d) enlarged local structure showing Me_2NH_2^+ viewed along the *a* and *b* axes, respectively. Note: the structure of UPC-H5a is illustrated using the crystal data of UPC-H5 owing to the slight change of the structure as indicated by PXRD tests.

directions, Fig. 4b–d. Therefore, partial replacement of the Me_2NH_2^+ groups by NH_4^+ with tetrahedral N–H configuration in $\text{UPC-H5a@NH}_3 \cdot \text{H}_2\text{O}$ further promotes the formation of smooth proton transfer pathways, resulting in further optimization of the proton conducting properties. In addition, NH_4^+ with the lower $\text{p}K_{\text{a}}$ value (9.26) and smaller volume enables $\text{UPC-H5a@NH}_3 \cdot \text{H}_2\text{O}$ to donate more protons and provide a larger pore volume as demonstrated by gas uptake tests in comparison with Me_2NH_2^+ ($\text{p}K_{\text{a}} = 10.75$), enriching more free water molecules and further forming more smooth proton transfer pathways. This also contributes to the optimized proton conducting functionality for $\text{UPC-H5a@NH}_3 \cdot \text{H}_2\text{O}$. Free water molecules enter into the channels of $\text{UPC-H5a@NH}_3 \cdot \text{H}_2\text{O}$ and form proton conduction pathways together with ammonium ions, which can be well confirmed by the measurements of the proton conductivity of the single $\text{UPC-H5a@NH}_3 \cdot \text{H}_2\text{O}$ crystal, Fig. S19.† As shown in Fig. 4a and S11,† the single crystal of UPC-H5 does not form successive hydrogen bonds along the [001] direction (*c* axis). However, the proton conductivity of the single $\text{UPC-H5a@NH}_3 \cdot \text{H}_2\text{O}$ crystal along the [001] direction is $1.67 \times 10^{-1} \text{ S cm}^{-1}$, which is similar to the value ($1.59 \times 10^{-1} \text{ S cm}^{-1}$) of the $\text{UPC-H5a@NH}_3 \cdot \text{H}_2\text{O}$ pellet, but much larger than the value ($6.88 \times 10^{-3} \text{ S cm}^{-1}$) along the [100] direction that has continuous hydrogen bonds initially, indicating the formation of smooth proton conduction pathways along the [001] direction in $\text{UPC-H5a@NH}_3 \cdot \text{H}_2\text{O}$. It should be noted that $\text{UPC-H5a@NH}_3 \cdot \text{H}_2\text{O}$ has the higher proton conductivity but the bigger activation energy. This is because NH_4^+ with a tetrahedral N–H configuration and the lower $\text{p}K_{\text{a}}$ value can form more hydrogen bonds and stronger host–guest interactions with the framework, hindering its reorientation and increasing the activation energy. The bigger activation energy should result in lower proton conductivity, but this unfavorable factor is offset by more available free protons donated by NH_4^+ and more

smooth proton transfer pathways formed by NH_4^+ and more water molecules, leading to high proton conductivity.^{11a}

In summary, a porous HOF with a high density of $-\text{PO}_3\text{H}$, Me_2NH_2^+ and H_2O and a characteristic tunable structure was constructed based on a phosphonate-based porphyrin nickel building block. This material exhibits guest-responsive proton conductivity. In particular, the ammonia-exchanged material shows high proton conductivity in a wide temperature range, up to $1.59 \times 10^{-1} \text{ S cm}^{-1}$ at 80°C and 99% R.H., representing one of the highest values among the excellent porous proton-conducting materials reported thus far. The result demonstrates that guest regulation is an effective method to improve the proton conductivity of HOF-based materials. This is surely helpful in designing and developing new HOF-based proton conductors with excellent performance.

Conflicts of interest

There are no conflicts to declare.

Acknowledgements

This work was financially supported by the National Natural Science Foundation of China (No. 21771193, 21631003, and 21875285), Taishan Scholar Foundation (No. ts201511019), Key Research and Development Projects of Shandong Province (2019JZZY010331), and Fundamental Research Funds for the Central Universities (No. 18CX05020A).

Notes and references

- 1 Y. Peng, G. Xu, Z. Hu, Y. Cheng, C. Chi, D. Yuan, H. Cheng and D. Zhao, *ACS Appl. Mater. Interfaces*, 2016, **8**, 18505–18512.
- 2 P. Kallem, N. Yanar and H. Choi, *ACS Sustainable Chem. Eng.*, 2019, **7**, 1808–1825.
- 3 S. Sharma and S. K. Ghoshal, *Renewable Sustainable Energy Rev.*, 2015, **43**, 1151–1158.
- 4 (a) S. Zhang, Y. Lu, X. Sun, Z. Li, T. Dang, Z. Zhang, H. Tian and S. Liu, *Chem. Commun.*, 2020, **56**, 391–394; (b) X. Meng, H. Wang, S. Song and H. Zhang, *Chem. Soc. Rev.*, 2017, **46**, 464–480; (c) Y. Wei, X. Hu, Z. Han, X. Dong, S. Zang and T. C. W. Mak, *J. Am. Chem. Soc.*, 2017, **139**, 3505–3512; (d) R. E. Rosli, A. B. Sulong, W. R. W. Daud, M. A. Zulkifley, T. Husaini, M. I. Rosli, E. H. Majlan and M. A. Haque, *Int. J. Hydrogen Energy*, 2017, **42**, 9293–9314.
- 5 (a) A. Li, Q. Gao, J. Xu and X. Bu, *Coord. Chem. Rev.*, 2017, **344**, 54–82; (b) S. Bao, G. K. H. Shimizu and L. Zheng, *Coord. Chem. Rev.*, 2019, **378**, 577–594.
- 6 Y. Yang, X. He, P. Zhang, Y. H. Andaloussi, H. Zhang, Z. Jiang, Y. Chen, S. Ma, P. Cheng and Z. Zhang, *Angew. Chem., Int. Ed.*, 2020, **59**, 3678–3684.
- 7 (a) N. T. T. Nguyen, H. Furukawa, F. Gándara, C. A. Trickett, H. M. Jeong, K. E. Cordova and O. M. Yaghi, *J. Am. Chem. Soc.*, 2015, **137**, 15394–15397; (b) S. M. Elahi, S. Chand, W. Deng, A. Pal and M. C. Das, *Angew. Chem., Int. Ed.*, 2018, **57**, 6662–6666; (c) P. Ramaswamy, N. E. Wong and

- G. K. H. Shimizu, *Chem. Soc. Rev.*, 2014, **43**, 5913–5932; (d) B. Joarder, J. Lin, Z. Romero and G. K. H. Shimizu, *J. Am. Chem. Soc.*, 2017, **139**, 7176–7179; (e) S. S. Bao, N. Li, J. M. Taylor, H. Kitagawa and L. Zheng, *Chem. Mater.*, 2015, **27**, 8116–8125; (f) S. Hwang, E. J. Lee, D. Song and N. C. Jeong, *ACS Appl. Mater. Interfaces*, 2018, **10**, 35354–35360; (g) Y. Wang, M. Zhang, Q. Yang, J. Yin, D. Liu, Y. Shang, Z. Kang, R. Wang, D. Sun and J. Jiang, *Chem. Commun.*, 2020, **56**, 15529–15532; (h) Q. Liu, Z. Li, D. Wang, Z. Li, X. Peng, C. Liu and P. Zheng, *Front. Chem.*, 2020, **8**, 694.
- 8 (a) Z. Meng, A. Aykanat and K. A. Mirica, *Chem. Mater.*, 2019, **31**, 819–825; (b) H. S. Sasmal, H. B. Aiyappa, S. N. Bhange, S. Karak, A. Halder, S. Kurungot and R. Banerjee, *Angew. Chem., Int. Ed.*, 2018, **57**, 10894–10898.
- 9 (a) S. Chand, S. M. Elahi, A. Pal and M. C. Das, *Chem. - Eur. J.*, 2019, **25**, 6259–6269; (b) Y. Tian, G. Liang, T. Fan, J. Shang, S. Shang, Y. Ma, R. Matsuda, M. Liu, M. Wang, L. Li and S. Kitagawa, *Chem. Mater.*, 2019, **31**, 8494–8503; (c) C. Yin, J. Li, Y. Zhou, H. Zhang, P. Fang and C. He, *ACS Appl. Mater. Interfaces*, 2018, **10**, 14026–14035; (d) S. Bao, N. Li, J. M. Taylor, Y. Shen, H. Kitagawa and L. Zhen, *Chem. Mater.*, 2015, **27**, 8116–8125; (e) F. Yang, G. Xu, Y. Dou, B. Wang, H. Zhang, H. Wu, H. Zhou, J. Li and J. Chen, *Nat. Energy*, 2017, **2**, 877–883; (f) M. Sadakiyo, T. Yamada, K. Honda, H. Matsui and H. Kitagawa, *J. Am. Chem. Soc.*, 2014, **136**, 7701–7707; (g) P. G. M. Mileo, K. Adil, L. Davis, A. Cadiou, Y. Belmabkhout, H. Aggarwal, G. Maurin, M. Eddaoudi and S. Devautour-Vinot, *J. Am. Chem. Soc.*, 2018, **140**, 13156; (h) D. I. Kolokolov, D. Lim and H. Kitagawa, *Chem. Rec.*, 2020, **20**, 1297; (i) M. Wahiduzzaman, S. Nandi, V. Yadav, K. Taksande, G. Maurin, H. Chun and S. Devautour-Vinot, *J. Mater. Chem. A*, 2020, **8**, 17951.
- 10 (a) W. J. Phang, H. Jo, W. R. Lee, J. H. Song, K. Yoo, B. S. Kim and B. S. Hong, *Angew. Chem.*, 2015, **127**, 5231–5235; (b) D. Umeyama, S. Horike, M. Inukai, T. Itakura and S. Kitagawa, *J. Am. Chem. Soc.*, 2012, **134**, 12780–12785; (c) Y. Tian, G. Liang, T. Fan, S. Shang, Y. Ma, R. Matsuda, M. Liu, M. Wang, L. Li and S. Kitagawa, *Chem. Mater.*, 2019, **31**, 8494–8503.
- 11 (a) S. Kim, B. Joarder, J. A. Hurd, J. Zhang, K. W. Dawson, B. S. Gelfand, N. E. Wong and G. K. H. Shimizu, *J. Am. Chem. Soc.*, 2018, **140**, 1077–1082; (b) F. Zhang, L. Dong, J. Qin, W. Guan, J. Liu, S. Li, M. Lu, Y. Lan, Z. Su and H. Zhou, *J. Am. Chem. Soc.*, 2017, **139**(17), 6183–6189; (c) K. C. Ranjesh, R. Illathvalappil, S. D. Veer, J. Peter, C. Wakchaure, K. V. Raj, S. Kurungot and S. S. Babu, *J. Am. Chem. Soc.*, 2019, **141**, 14950–14954; (d) Y. Yang, X. He, P. Zhang, Y. H. Andaloussi, H. Zhang, Z. Jiang, Y. Chen, S. Ma, P. Cheng and Z. Zhang, *Angew. Chem.*, 2020, **132**, 3707–3713.
- 12 (a) T. Yamada, K. Ostubo, R. Makiura and H. Kitagawa, *Chem. Soc. Rev.*, 2013, **42**, 6655–6669; (b) M. K. Sarango-Ramírez, D. Lim, D. I. Kolikolov, A. E. Khudozhitkov, A. G. Stepanov and H. Kitagawa, *J. Am. Chem. Soc.*, 2020, **142**, 6861–6865.
- 13 T. Grancha, J. Ferrando-Soria, J. Cano, P. Amorós, B. Seoane, J. Gascon, M. Bazaga-García, E. R. Losilla, A. Cabeza and D. Armentano, *Chem. Mater.*, 2016, **28**, 4608–4615.
- 14 (a) M. Bazaga-García, R. M. P. Colodrero, M. Papadake, P. Garczarek, J. Zon, P. Olivera-Pastor, E. R. Losilla, L. León-Reina, M. A. G. Aranda, D. Choquesillo-Lazate, K. D. Demadis and A. Cabeza, *J. Am. Chem. Soc.*, 2014, **136**, 5731–5739; (b) R. Liu, L. Zhao, S. Yu, X. Liang, Z. Li and G. Li, *Inorg. Chem.*, 2018, **57**, 11560–11568; (c) R. Liu, Y. Liu, S. Yu, C. Yang, Z. Li and G. Li, *ACS Appl. Mater. Interfaces*, 2019, **11**, 1713–1722; (d) D. Lim, M. Sadakiyo and H. Kitagawa, *Chem. Sci.*, 2019, **10**, 16–33.
- 15 (a) S. Feng, Y. Shang, Z. Wang, Z. Kang, R. Wang, J. Jiang, L. Fan, W. Fan, Z. Liu, G. Kong, Y. Feng, S. Hu, H. Guo and D. Sun, *Angew. Chem., Int. Ed.*, 2020, **59**, 3840–3845; (b) Y. Li, E. V. Alexandrov, Q. Yin, L. Li, Z. Fang, W. Yuan, D. M. Proserpio and T. Liu, *J. Am. Chem. Soc.*, 2020, **142**, 7218–7224.
- 16 (a) T. Adachi and M. D. Ward, *Acc. Chem. Res.*, 2016, **49**, 2669–2679; (b) B. Han, H. Wang, C. Wang, H. Wu, W. Zhou, B. Chen and J. Jiang, *J. Am. Chem. Soc.*, 2019, **141**, 8737–8740.
- 17 R. Lin, Y. He, P. Li, H. Wang, W. Zhou and B. Chen, *Chem. Soc. Rev.*, 2019, **48**, 1362–1389.
- 18 J. Luo, J. Wang, J. Zhang, S. Lai and D. Zhong, *CrystEngComm*, 2018, **20**, 5884–5898.
- 19 (a) A. Karmakar, R. Illathvalappil, B. Anothumakkool, A. Sen, P. Samanta, A. V. Desai, S. Kurungot and S. K. Ghosh, *Angew. Chem., Int. Ed.*, 2016, **128**, 10825–10829; (b) G. Xing, T. Yan, S. Das, T. Ben and S. Qiu, *Angew. Chem., Int. Ed.*, 2018, **57**, 5345–5349; (c) Y. Qin, T. Gao, W. Xie, Z. Li and G. Li, *ACS Appl. Mater. Interfaces*, 2019, **11**, 31018–31027; (d) S. Chand, S. C. Pal, A. Pal, Y. Ye, Q. Lin, Z. Zhang, S. Xiang and M. C. Das, *Chem. - Eur. J.*, 2019, **25**, 1691–1695; (e) W. Yang, F. Yang, T. Hu, S. C. King, H. Wang, H. Wu, W. Zhou, J. Li, H. D. Arman and B. Chen, *Cryst. Growth Des.*, 2016, **16**, 5831–5835; (f) Q. Yang, Y. Wang, Y. Shang, J. Du, J. Yin, D. Liu, Z. Kang, R. Wang, D. Sun and J. Jiang, *Cryst. Growth Des.*, 2020, **20**, 3456–3465; (g) S. Chand, S. C. Pal, A. Pal, Y. Ye, Q. Lin, Z. Zhang, S. Xiang and M. C. Das, *Chem. - Eur. J.*, 2019, **25**, 1691–1695; (h) M. Yoon, K. Suh, H. Kim, Y. Kim, N. Selvapalam and K. Kim, *Angew. Chem., Int. Ed.*, 2011, **50**, 7870–7873; (i) Z. Sun, Y. Li, Z. Zhang, Z. Li, B. Xiao and G. Li, *New J. Chem.*, 2019, **43**, 10637.
- 20 A. L. Spek, *J. Appl. Crystallogr.*, 2003, **36**, 7–13.